# An Analysis of the Surface Breakup Mechanism of a Liquid Jet in Cross-flow

M. Behzad, N. Ashgriz*
Department of Mechanical and Industrial Engineering, University of Toronto, Canada
m.behzad.jazi@mail.utoronto.ca and ashgriz@mie.utoronto.ca

**Abstract**

The surface breakup of a liquid jet injected into a gaseous cross-flow is observed in moderate to high gas Weber number conditions which normally occur in the combustion applications. Although many experimental studies on the breakup regimes, the mechanism of jet surface breakup has not been fully understood because of difficulties to capture the near nozzle breakup phenomena. This study aims at providing useful observations regarding the fundamental physics involved in the surface breakup mechanism of a liquid jet in cross-flow in relatively high Weber number, using detailed numerical simulations. The results show that infinitesimal disturbances are excited immediately after the jet is exposed to the gas flow. As the disturbances are transported along the jet trajectory, they start to grow due to the shear instability. Subsequently a two-stage mechanism causes the jet surface to break up. In the first stage, the cross-flow drags the crests of waves in the downstream direction, which results in formation of sheet-like structures protruding to the leeward of the jet. In the second stage, the sheet surrounded by a thick rim, disintegrates into ligaments and finally droplets due to the propagation of span-wise waves.

## Introduction

The atomization of a non-turbulent liquid jet injected into a subsonic gaseous cross-flow consists of two parts: (1) primary breakup and (2) secondary breakup. Many experimental studies have been carried out over decades in order to capture several complexities involved in the primary breakup. According to these observations, two distinct mechanisms for the jet primary breakup have been recognized; the so called column breakup and surface breakup. In the column breakup mechanism, the entire liquid jet undergoes disintegration into large liquid lumps. In the surface breakup regime, liquid fragments such as ligaments and drops are separated from the jet surface before the column breakup occurs. Subsequently, the resulting ligaments and drops from two mentioned mechanisms break up into small droplets during the process of secondary breakup. The present study uses numerical simulations to provide some useful insights regarding the surface breakup mechanism of a non-turbulent liquid jet in cross-flow. It is restricted on the atomization of a *non-turbulent* jet in which the aerodynamic forces are the sole cause of the jet atomization.

## Surface/Shear Breakup Regime

The surface breakup of the jet is usually observed in high gas Weber number conditions ($\mathrm{We}_g > 100$) and is conventionally called the shear breakup. According to the experimental investigations, in the shear breakup mode ligaments and drops are stripped off the jet surface, mostly from the leeward side rather than windward [1],[2]. It is reported that the shear effect of the gas flow surrounding the jet periphery causes this type of breakup and thus it is named shear breakup. This breakup mode has been originally recognized for the secondary breakup of drops subjected to shock-waves [3]. Due to this analogy, the phenomenological analyses for the secondary breakup of a single droplet, have also been applied to model the surface breakup of a liquid jet in crossflow as it will be discussed in the following.

### *Shear Breakup Models*

One of the common models for shear breakup was developed theoretically based on experimental observations of drops exposed to shock-wave by Ranger and Nicholls [5]. They assumed that the *shear action* of the high-velocity gas flow on the drop surface causes the formation of two boundary layers outside and inside of the liquid drop as shown in Fig. 1 by dash lines. Thereafter, the liquid boundary layer is being stripped off the equator, due to its momentum, which leads to the droplets shear breakup. They finally presented a relation for mass removal rate from the periphery of a parent drop.

Hsiang and Faeth presented a similar concept to the Boundary Layer Stripping (BLS) model [10]. They concluded that during the shear breakup, the droplets are shedding from the circumference of the parent drop

*Corresponding author: ashgriz@mie.utoronto.ca

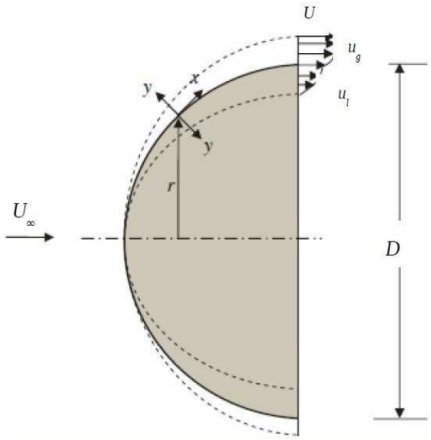


**Figure 1.** Boundary Layer Stripping (BLS) Model. $x$ is the curvilinear coordinate along the interface and $y$ is the coordinate perpendicular to the interface [6].

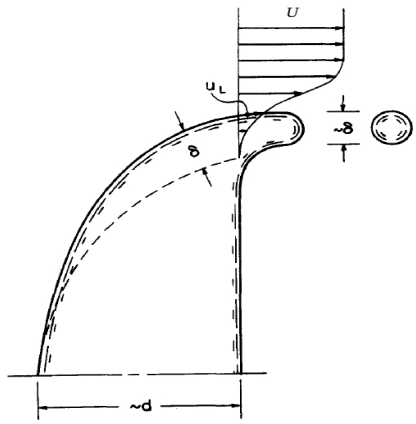


**Figure 2.** Sketch of the shear breakup mechanism [10].

due to formation of a boundary layer inside the liquid surface. Therefore, they assumed that the thickness of the boundary layer as it reaches the drop periphery is proportional to the Sauter Mean Diameter (SMD) of drops currently being formed, i.e. SMD$(t) \sim \delta(t)$. Figure. 2 illustrates the flow configuration of their analysis. It shows a deformed parent drop at the onset of droplets formation from the drop edge. Chou et al. extended the previous assumption by suggesting two basic types of behaviors: (1) a transient regime where there is a progressive increase of boundary layer thickness (and thus droplet diameter) with the time, and (2) a regime where the boundary layer thickness is relatively independent of time [3]. Accordingly, they introduced two sets of correlations for the size of produced ligaments and droplets.

***Application of Models to Jet Surface Breakup***

Having modified the BLS model, it has been applied to the shear breakup mechanism of a liquid jet. The first modification was to increase the droplet shedding rate linearly with distance away from injection location [7]. This may account for the lack of shedding close to the injection location and the subsequent build-up of shedding over the life of liquid column. Mashayek et al. [9] also modified the BLS model by taking into account the mass shedding from a 2-D cylindrical jet element instead of a axisymmetric liquid drop.

Sallam et al. [4] employed a pulsed holography technique to penetrate the dense spray region and observed the surface breakup properties of a liquid jet. They proposed a boundary layer concept similar to Hsiang and Faeth's assumption for modeling the jet surface breakup. According to their observations, the appearance of drops was always preceded by the formation of ligaments stretching toward the lee-side of the jet. They also assumed that liquid motion required to form a ligament, is originated from the viscous shear layer. This layer begins at the jet windward side and grows toward its periphery due to the shear forces of the gas flow field. In order to incorporate the two mentioned regimes, previously observed for the droplet breakup, they considered the jet as a 2-D droplet with initial diameter $D_j$ that travels with jet initial velocity $U_j$, along its trajectory. Therefore, the temporal variation of boundary layer thickness is replaced with spatial as $t = z/U_j$, where $z$ is the distance that the 2-D element reaches from injection point. Similar to the droplet shear breakup, the droplet diameter is assumed to be proportional to the boundary layer thickness at any distance $z$, i.e. $SMD(z) \sim \delta(z)$.

In summary, in the above-mentioned models the underlying assumption is based on the *viscous* theory which states that laminar boundary layers in both liquid and gas phases are formed. However, there are several studies that question the viscous interpretation of surface breakup [6],[12],[8]. For instance, Liu and Reitz proposed sheet-thinning mechanism in which the edges of the saucer-shaped drop are drawn out into a thin sheet by the gas inertia, and then the sheet is split up into ligaments [12]. In addition numerical simulations of inviscid accelerated drops show essentially the same behavior as viscous drops, supporting an inviscid breakup mechanism [13]. Nevertheless, to the knowledge of authors, there is no *inviscid* model to predict the size distribution of the droplets produced by surface breakup.

The goal of current study is to observe and understand the jet surface breakup mechanism more comprehensively.

**Numerical Methods**

In the present study, Large Eddy Simulation (LES) of a non-turbulent liquid jet injected into a cross-flow is performed using TransAT code [14]. The computational domain consists of a 2-D channel with inflow-outflow boundary condition in stream-wise direction ($x$), symmetry in span-wise ($y$) and no-slip condition in wall-normal ($z$) direction. To estimate the domain size the following trajectory correlation is used

$$\frac{z_b}{D_j} = \sqrt{\frac{\pi}{C_D}}\sqrt{\frac{qx_b}{D_j}} \tag{1}$$

$q$ is the momentum flux ratio defined as $\rho_l U_j^2/\rho_g U_g^2$ where, $U_g$ and $U_j$ are the mean gas and jet velocity and, $\rho_l$ and $\rho_g$ are the liquid and gas density respectively. The column breakup point denoted by $b$ is located approximately at $x_b = 8D_j$ downstream of the jet injection point, and the modified drag coefficient $C_D$ is 3 [4]. Thus the dimensions of the domain are chosen as $16D_j$, $8D_j$, and $10D_j$ in $x$, $y$, and $z$ direction respectively. The minimum mesh size is 10 $\mu m$ in the vicinity of the injection point and it is gradually increased by a ratio of 1.02 in all directions.

The jet velocity profile is calculated by the 1/7-power law approximation with a mean value of $U_j$. The gas velocity profile of the channel inflow resembles a mean fully developed turbulent profile and it remains steady during the simulation. Thus the velocity fluctuations of gas inflow profile are not considered which enables us to take into account the sole effect of gas aerodynamic forces and neglect the turbulent effects on the breakup and deformation of the jet. In other words, any effects that might be observed will be due to the aerodynamic action of gas flow.

A single set of mass and momentum balance equations are solved for the whole computational domain using an incompressible fluid with variable material properties as follows

$$\frac{\partial u_j}{\partial x_j} = 0 \tag{2}$$

$$\frac{\partial u_i}{\partial t} + \frac{\partial}{\partial x_j}(u_i u_j) = \frac{1}{\rho}\frac{\partial}{\partial x_j}(-p\delta_{ij} + \tau_{ij}) + \sigma\kappa\delta^I n_i \tag{3}$$

where $u_i$ is the velocity vector, $p$ is the pressure, $\sigma$ is the surface tension coefficient, $\kappa$ is the interface curvature, $n_i$ is the normal vector, $\delta^I$ is a smoothed Dirac delta function centered at the interface and $\delta_{ij}$ is the Kronecker delta. $\tau_{ij}$ is the shear stress tensor representing by the following expression for Newtonian fluids

$$\tau_{ij} = 2\mu S_{ij} \qquad where \qquad S_{ij} = \frac{1}{2}(\frac{\partial u_i}{\partial x_j} + \frac{\partial u_j}{\partial x_i}) \tag{4}$$

Turbulence in each phase of the flow is modeled using a Smagorinsky Large Eddy Simulation (LES), however, none of the sub-grid terms arising from filtering the interface are modeled. The approach instead relies on resolving all relevant scales at the interface.

The phase interface is captured by the level set method in which the level set function, $\Phi(x_i, t)$, is defined as a smooth signed-distance function referring to the shortest distance to the interface front. It has negative values in gas and positive values in liquid phase and the interface is indicated by zero level set function, i.e. $\Gamma = \{x_i|\Phi(x_i, t) = 0\}$. Since the distance function is a material property, it is advected by the flow-field as follows

$$\frac{\partial \Phi}{\partial t} + u_j\frac{\partial \Phi}{\partial x_j} = 0 \tag{5}$$

Consequently, the normal vector and the curvature of the interface can easily be expressed in terms of $\phi(x_i, t)$

$$\boldsymbol{n} = (\frac{\boldsymbol{\nabla}\Phi}{|\boldsymbol{\nabla}\Phi|})_{\Phi=0} \qquad and \qquad \kappa = \boldsymbol{\nabla}.\boldsymbol{n} \tag{6}$$

A modified Heaviside function, based on the level set functions, is employed to smooth the physical properties of fluids across the interface with a thickness of $2\epsilon$ and it is defined as

$$H_\epsilon(\Phi) = \frac{1}{2}(1 + \tanh\frac{2\Phi}{\epsilon}) \tag{7}$$

Therefore, the fluid properties are determined based on the interface location, using

$$\rho(x_i, t) = \rho_g + (\rho_l - \rho_g)H_\epsilon(\Phi(x_i, t)) \qquad and \qquad \mu(x_i, t) = \mu_g + (\mu_l - \mu_g)H_\epsilon(\Phi(x_i, t)) \tag{8}$$

and the Dirac delta function is smoothed as

$$\delta^I(\Phi) = \frac{\mathrm{d}H_\epsilon}{\mathrm{d}\Phi} \tag{9}$$

Although $\Phi(x_i, 0)$ is a distance function, it will not necessarily remain one under the evolution of Eq. (5). Thus, there is a reintilization step during which a level set function is a distance function without changing its zero level set [11].

**Results and Discussion**

The conditions and flow properties of the simulation is summarized in table 1. Figures 3 and 4 depict evolution of a liquid jet interface ($\Phi(x_i, t) = 0$) in cross-flow condition. As shown in the figures, liquid particles including droplets and ligaments with various shapes and sizes are separating from the jet body. Two different breakup

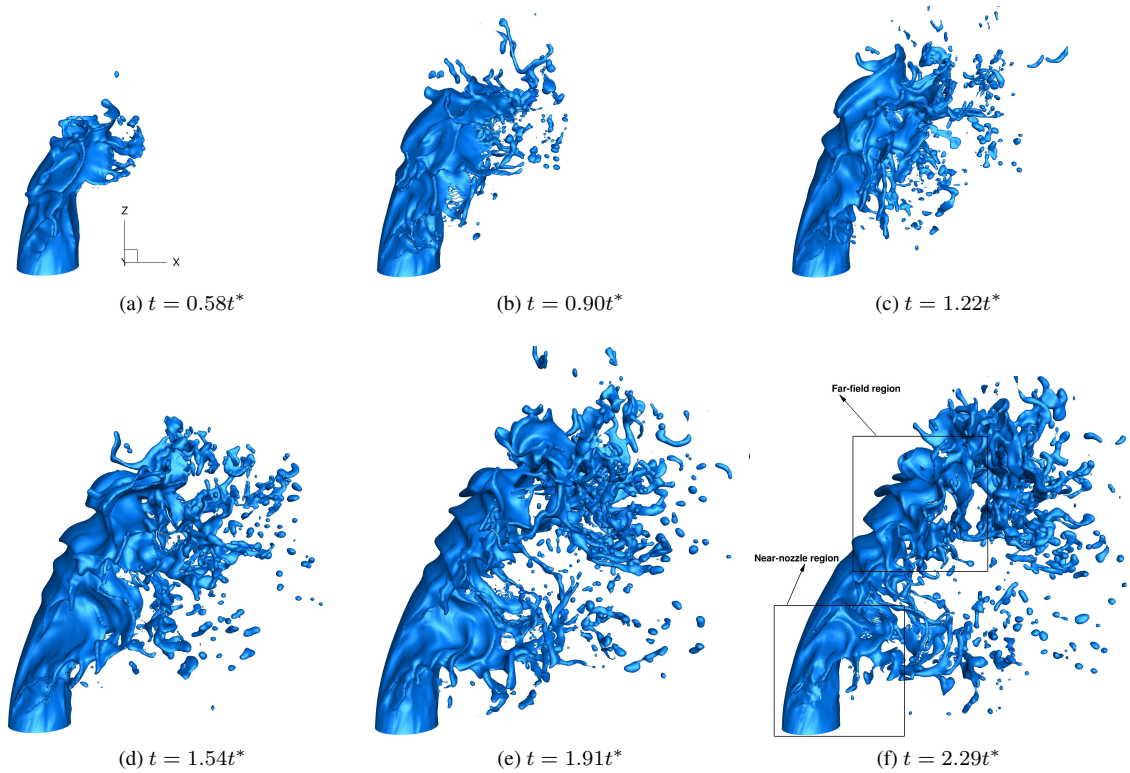


(a) $t = 0.58t^*$ (b) $t = 0.90t^*$ (c) $t = 1.22t^*$

(d) $t = 1.54t^*$ (e) $t = 1.91t^*$ (f) $t = 2.29t^*$

**Figure 3.** Evolution of a jet in cross-flow, side views (X-Z).

regions may be recognized in these figures (see e.g. Fig. 3.f). The near-field region (close to the injection point) in which small-scale phenomena such as short-wave disturbances and surface breakup exist, and the far-field region (near the end of jet trajectory) where the larger-scale phenomena such as windward surface waves lead to disintegration of entire jet body to relatively large particles. Since the goal of the present simulations is to study the jet surface breakup process, we focus to the near-nozzle region where the surface breakup originally occurs.

Two specific cross-sections of the jet at the near-nozzle region are shown in Fig. 5. The vectors represent resultant velocities of the jet velocity components in $x$ and $y$ directions, which physically imply the deviation of the streamlines originated from the jet inflow toward the sides. The pressure variation at the jet circumference (high pressure at the windward zone and low pressure at the sides) deforms the cylindrical interface of the jet to a roughly elliptical one. As a result of this deformation a flow tendency toward the jet sides are created. Therefore, it can be concluded that the aerodynamic pressure, i.e. form drag, is the main cause of inducing such a flow-field at this high Reynolds number. This is often neglected in the viscous interpretation of jet surface breakup which assume that only the shear forces of the gas flow provide the liquid motion inside the jet for the breakup.

Figure 6 shows a close-up of the jet interface at the near-nozzle region. Besides the global deformation of the jet cross-section discussed earlier, there are two distinct wave-like structures on each side of the jet windward

**Table 1.** Flow properties and characteristic numbers of the simulation.

| | Value | | Value |
|---|---|---|---|
| Jet exit diameter $D_j$ (mm) | 0.5 | Liquid surface tension (N/m) | 0.005 |
| Channel half width $\delta = 5D_j$ (mm) | 2.5 | Characteristic breakup time ($t^* = D_j/U_g(\rho_l/\rho_g)^{0.5}$) (s) | $3.95 \times 10^{-5}$ |
| Cross-flow mean velocity $U_g$ (m/s) | 40 | Momentum flux ratio $q$ | 10 |
| Jet mean velocity $U_j$ (m/s) | 40 | Ohnesorge number (Oh $= \mu_l/(\rho_l \sigma D_j)^{0.5}$) | 0.01825 |
| Gas density (kg/m$^3$) | 1.2 | Gas Weber number (We$_g = \rho_g U_g^2 D_j/\sigma$) | 192 |
| Density ratio ($\rho_l/\rho_g$) | 10 | Jet Weber number (We$_j = \rho_l U_j^2 D_j/\sigma$) | 1920 |
| Gas dynamic viscosity (Pa.s) | $1.0 \times 10^{-5}$ | Jet Reynolds number (Re$_j = \rho_l U_j D_j/\mu_l$) | 2400 |
| Liquid dynamic viscosity (Pa.s) | $1.0 \times 10^{-4}$ | Channel Reynolds number (Re$_\delta = \rho_g U_g 2\delta/\mu_g$) | 24000 |

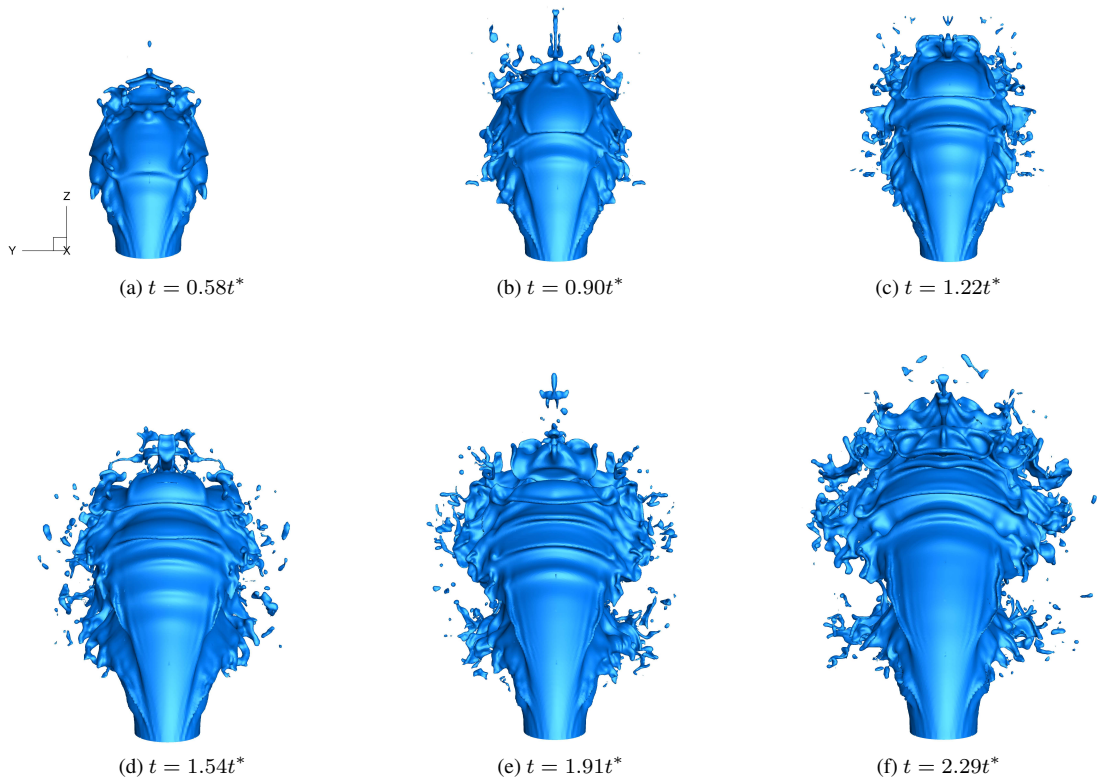


(a) $t = 0.58t^*$ (b) $t = 0.90t^*$ (c) $t = 1.22t^*$

(d) $t = 1.54t^*$ (e) $t = 1.91t^*$ (f) $t = 2.29t^*$

**Figure 4.** Evolution of a jet in cross-flow, back views (Y-Z).

surface which are triggered immediately after the jet is exposed to the cross-flow. The birth of such disturbances might be due to the jet pressure fluctuations produced by the cross-flow, or it may be originated numerically. To investigate more, several cross-sections of the jet at various distances from the nozzle are again plotted in Fig. 7. The zero and 180 degree indicate the leeward and windward of the jet surface which is non-dimensionalized by the jet initial diameter $D_j$ relative to the cross-section centroid. As can be seen in this figure, the amplitude of disturbances tends to grow in $z$ direction. The reason for such growing can be possibly explained in the context of the shear instability. After cross-flow reaches the stagnation point on the jet surface ($\theta = 180$), it begins to accelerate toward the jet periphery ($\theta = 90, 270$). Therefore, the velocity in azimuthal direction ($\theta$ component) varies continuously across the interface in radial direction, from far-filed potential gas velocity to nearly zero velocity inside the jet. As a result of such velocity variation, the interface is susceptible to shear instability, leading to the growth of the infinitesimal disturbances. The disturbances are also slightly moving in azimuthal direction toward the jet periphery, and are eventually dragged out of the jet body as sheets to the downstream direction by the gas cross-flow. Furthermore, span-wise waves begin to propagate on these sheets. The waves cause the sheets

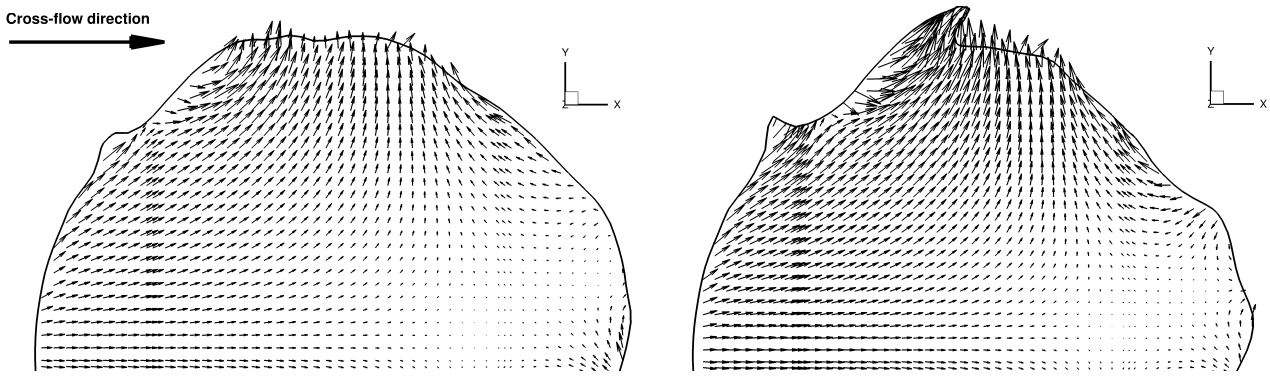


(a) $z = 0.3D_j$ (b) $z = 0.4D_j$

**Figure 5.** Cross-sections of half of the jet at $t = 1.54t^*$.

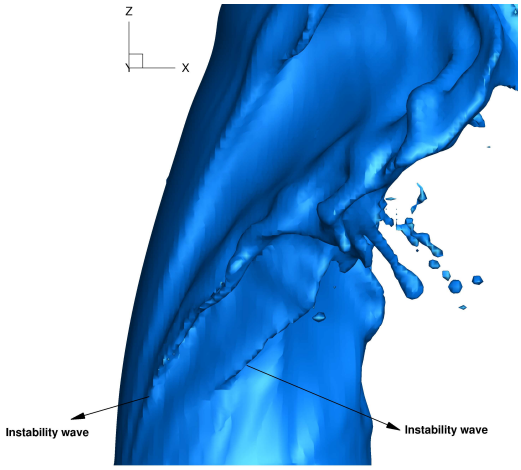


(a) Side view (X-Z plane)

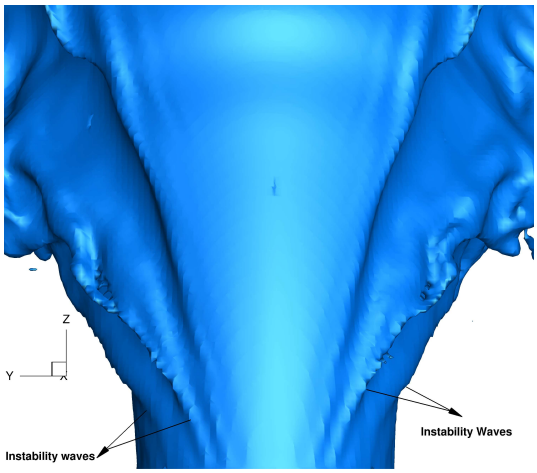


(b) Back view (Y-Z plane)

**Figure 6.** Close-up views of the near nozzle region

to become thin membranes in between them with a enclosing thick rim. The thin liquid membranes subsequently burst, forming small droplets, while the waves produce span-wise ligaments which either separate from the jet body or break up into relatively larger drops.

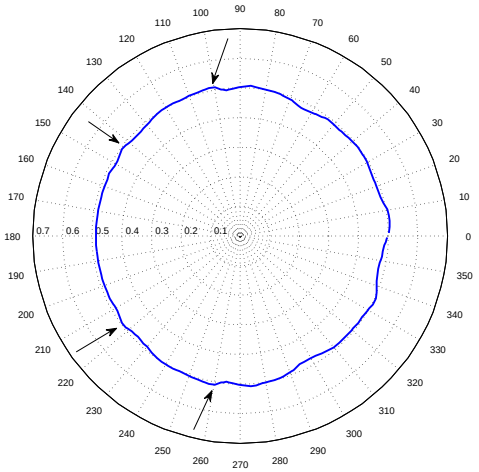


(a) $z = 0.2D_j$

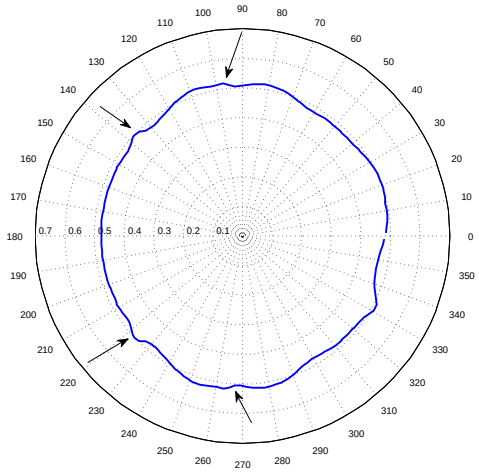


(b) $z = 0.3D_j$

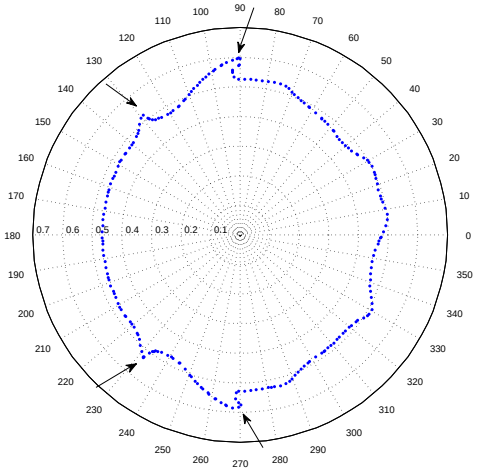


(c) $z = 0.4D_j$

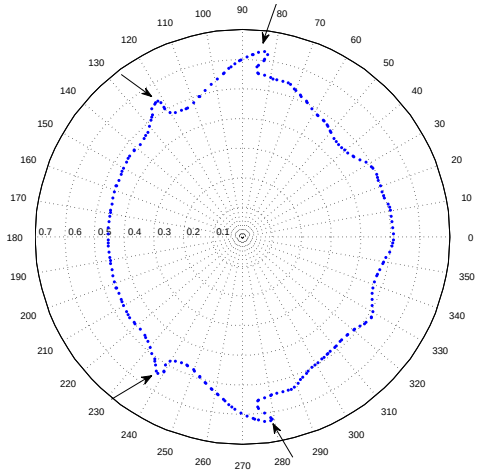


(d) $z = 0.5D_j$

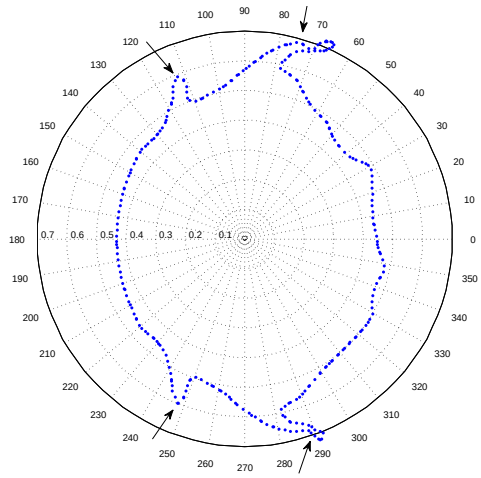


(e) $z = 0.6D_j$

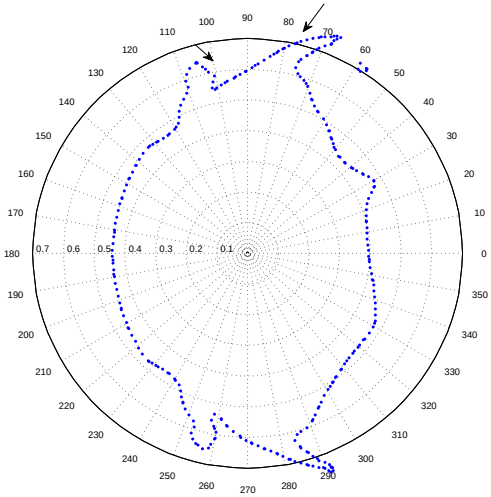


(f) $z = 0.7D_j$

**Figure 7.** Cross-sections of the jet at $t = 1.54t^*$. The arrows show the position of disturbances.

## Conclusions

Detailed numerical simulation is performed to extend our knowledge of the liquid jet surface breakup mechanism in cross-flow conditions. A new explanation for the jet surface breakup is provided based on the shear instability concept at the jet surface. Accordingly. the gas-liquid interface at the near-nozzle region become unstable due to the existence of an azimuthal velocity variation in radial direction. The instabilities then grow in amplitude and are pulled out into downstream of the jet as sheet-like structures by the aerodynamic pressure. The sheets then undergo breakup into ligaments by the action of span-wise waves. Despite the fact that inviscid interpretations of the jet surface breakup ignore the shear effect on the liquid surface (jet and drop), we observed that a velocity gradient (a viscous effect) near the interface can cause a well-defined mechanism for initiation of the jet surface breakup.

## Acknowledgments

The study is sponsored by Ontario Research Fund (ORF) and Natural Sciences and Engineering Research Council of Canada (NSERC). The simulations are being performed using TransAT code developed at ASCOMP GmbH company [14] and SciNet High Performance Computational Resources [15].

## References

[1] Mazallon, J., Dai, Z. and Faeth, G.M. *Atomization and Sprays* 9(3):291-311 (1999).
[2] Wu, P-K, Kirkendall, K.A., Fuller, R.P. and Nejad, A.S. *Journal of Propulsion and Power* 13(1):64-73 (1997).
[3] Chou, W.-H, Hsiang, L.-P. and Faeth, G.M. *Int. J. Multiphase Flow* 23(4):651-669 (1997).
[4] Sallam, K.A., Aalburg, C. and Faeth, G.M. *AIAA Journal* 42(12):2529-2540 (2004).
[5] Ranger A.A. and Nicholls, J.A. *AIAA Journal* 7(2):285-290 (1969).
[6] Guildenbecher, D.R., Lopez-Rivera, C. and Sojka, P.E. *Experiments in Fluids* 46(3):371-402 (2009).
[7] Khosla, S. and Crocker, D.S. *Proc. ASME Turbo Expo, Vienna, Austria, 2011*.
[8] Khosla, S., Smith, C.E. and Throckmorton, R.P. *$19^{th}$ ILASS, Toronto, Canada, 2006*.
[9] Mashayek, A., Behzad, M. and Ashgriz, N. *AIAA Journal* 49(11):2407-2420 (2011).
[10] Hsiang, L.-P. and Faeth, G.M. *Int. J. Multiphase Flow* 18:635-652 (1992).
[11] Sussman, M., Fatemi, E., Smereka, P. and Osher, S. *Computers and fluids* 27(5-6):663-680 (1998).
[12] Liu, Z. and Reitz, R.D. *Int. J. Multiphase Flow* 23(4):631-650 (1997).
[13] Han, J. and Tryggvason, G. *Physics of Fluids* 13:1554-1565 (2001).
[14] http://www.ascomp.ch/
[15] http://www.support.scinet.utoronto.ca/wiki